Computer Assisted Methods in Engineering and Science
29(3): 179–195, 2022, doi: 10.24423/cames.459

A Meshless Pseudospectral Approach Applied to Problems with Weak Discontinuities

Artur KROWIAK

Institute of Computer Science, Mechanical Faculty, Cracow University of Technology, Cracow, Poland; e-mail: artur.krowiak@pk.edu.pl

In this paper, a meshless pseudospectral method is applied to solve problems possessing weak discontinuities on interfaces. To discretize a differential problem, a global interpolation by radial basis functions is used with the collocation procedure. This leads to obtaining the differentiation matrix for the global approximation of the differential operator from the analyzed equation. Using this matrix, the discretization of the problem is straightforward. To deal with the differential equations with discontinuous coefficients on the interface, the meshless pseudospectral formulation is used with the so-called subdomain approach, where proper continuity conditions are used to obtain accurate results. In the present paper, the differentiation matrix for this method is derived and the choice of a proper value of the shape parameter for radial functions in the context of the subdomain approach is studied. The numerical tests show the effectiveness of the method when using regular or unstructured node distribution. They confirm that the approach preserves well-known advantages of the radial basis function collocation method, i.e., rapid convergence, simplicity of the implementation and extends its usage for problems with weak discontinuity.

Keywords: RBF pseudospectral method, meshless method, interface problem, subdomain approach.

1. Introduction

In recent years, many formulations of meshless methods for solving differential equations have been developed [1, 2]. This is the result of their useful features, the most important of which is the possibility of the domain discretization by using scattered nodes. This simplifies the discretization of complex geometries and accelerates remeshing procedures. Among these methods, there is a wide variety of collocation techniques based on global radial basis function (RBF) interpolation. It was proved by several researchers [3, 4] that this type of base functions is particularly useful in scattered data interpolation and can be conveniently applied in higher dimensions.

Moreover, the global RBF collocation methods can exhibit exponential convergence [5], which is not achievable for low-order approximation techniques such as the finite difference method and finite element one. The global RBF collocation methods can be divided into two main categories: the so-called Kansa approach [6, 7] and the RBF pseudospectral method (RBF-PS) [8]. The first one solves the differential problem by giving the interpolant that approximates the solution, and therefore it can be considered an analytical-approximate approach. The second one gives numerical values of the solution at the nodes and is considered a purely numerical approach. There are many examples of applying these methods for solving engineering as well as scientific problems in several areas. A comprehensive overview can be found in [9].

Since the mentioned methods take advantage of infinitely smooth global base functions, they are dedicated to problems possessing smooth solutions. Many problems in science and engineering do not possess such solutions, e.g., diffusion in an element composed of different materials linked by an interface. Such a problem is modeled by a differential equation with discontinuous coefficients on the interface and is characterized by a non-smooth, continuous solution with a discontinuous derivative, which is called weak discontinuity.

Several numerical methods have been developed for such problems. Among them, some methods employ RBF interpolation. In [10], a localized version of the RBF method is presented, where the polynomial term of enriched RBF interpolant is adjusted to properly reflect the interface conditions. In other meshless methods [11, 12], a generalized moving least-squares approximation is combined with the visibility criterion technique to solve more general (nonhomogeneous) interface problems. All these methods can be classified as localized discretization techniques in contrast to the ones mentioned above.

To allow the Kansa method to be applicable to problems with weak discontinuity, the method has been combined with the so-called subdomain approach and successfully applied to a heat conduction problem as well as elasticity one [13, 14].

In some cases, it is more convenient to have purely numerical results at imposed nodes than to evaluate global interpolation function to obtain the value. This situation arises, for example, in non-linear problems, where some iterations of the discrete system are needed to obtain the approximate solution. In this case, many evaluations of global interpolant slow down the computational procedure, and therefore the pseudospectral method is a better choice. In the present paper, the formulation of the RBF-PS method for problems with a weak discontinuity is developed. To this end, the RBF-PS is combined with a subdomain approach. In the approach, the domain is divided into subdomains, in which the problem is homogeneous and proper continuity conditions are imposed at the interface nodes to accurately reflect a non-smooth solution. The procedure for determining

the differentiation matrix, which approximates the differential operator from the equation, is shown. With this matrix, the discretization of the problem is carried out. When one uses the RBF, careful attention has to be paid to the system's conditioning. The latter can be controlled by a shape parameter contained in the RBF. Two main algorithms for choosing a good parameter value are tested in the present paper in the context of the subdomain approach. The concluding remarks on the accuracy, stability and convergence are drawn based on results from the solution of ordinary and partial differential equations.

2. Radial basis function-based pseudospectral approach

Let us consider a boundary-value problem in a general form:

$$Lu = f \quad \text{in} \quad \Omega, \qquad Bu = g \quad \text{on} \quad \partial\Omega, \tag{1}$$

where L and B denote linear differential operators imposed on the sought function u in the domain Ω and on the boundary $\partial\Omega$, respectively, and f, g are known functions. In the RBF-PS method, the domain of the problem, including the boundary, can be represented by scattered nodes $\mathbf{x}_i$, $i = 1, ..., N$. Among them, one can distinguish between interior nodes $\mathbf{x}_i^I$, $i = 1, ..., N_I$ and the nodes imposed on the boundary $\mathbf{x}_i^B$, $i = 1, ..., N_B$. Using these nodes, the sought function is interpolated with the RBF as follows:

$$u_h(\mathbf{x}) = \sum_{j=1}^{N} \alpha_j \varphi\left(\|\mathbf{x} - \mathbf{x}_j\|\right), \tag{2}$$

where $\varphi_j(\mathbf{x}) = \varphi\left(\|\mathbf{x} - \mathbf{x}_j\|\right)$ is the RBF centered at the j-th node, and α_j is the interpolation coefficient.

In order to determine the differentiation matrix for the approximation of operators L and B two steps are needed. In the first one, the interpolation coefficients are expressed in terms of unknown function values u at the nodes. To this end, the interpolation conditions are introduced:

$$u_h(\mathbf{x}_i) = \sum_{j=1}^{N} \alpha_j \varphi\left(\|\mathbf{x}_i - \mathbf{x}_j\|\right) = u_i, \qquad i = 1, ..., N, \tag{3}$$

and solved with respect to coefficients α_j. It can be conveniently written in the matrix notation as:

$$\boldsymbol{\alpha} = \boldsymbol{\Phi}^{-1}\mathbf{u}, \tag{4}$$

where $\boldsymbol{\alpha} = \left[\begin{array}{ccc} \alpha_1 & \cdots & \alpha_N \end{array}\right]^T$, $\mathbf{u} = \left[\begin{array}{ccc} u_1 & \cdots & u_N \end{array}\right]^T$ and $\boldsymbol{\Phi}_{ij} = \varphi(\|\mathbf{x}_i - \mathbf{x}_j\|)$, $i, j = 1, ..., N$.

In the second step, the differential operators are imposed on interpolant (2) and evaluated at respective nodes, which yields:

$$\mathbf{u}_{LB} = \mathbf{\Phi}_{LB}\boldsymbol{\alpha}, \tag{5}$$

where the left-hand side of the above equation denotes the discrete values of the derivatives at respective nodes in the domain as well as on the boundary, and the $\mathbf{\Phi}_{LB}$ matrix (the so-called Kansa matrix) has the structure:

$$\mathbf{\Phi}_{LB} = \begin{bmatrix} \mathbf{\Phi}_L \\ \mathbf{\Phi}_B \end{bmatrix},$$

$$(\mathbf{\Phi}_L)_{ij} = \left[L\varphi\left(\|\mathbf{x} - \mathbf{x}_j\|\right)\right]_{\mathbf{x}=\mathbf{x}_i^I}, \qquad i = 1, ..., N_I, \quad j = 1, ..., N,$$

$$(\mathbf{\Phi}_B)_{ij} = \left[B\varphi\left(\|\mathbf{x} - \mathbf{x}_j\|\right)\right]_{\mathbf{x}=\mathbf{x}_i^B}, \qquad i = 1, ..., N_B, \quad j = 1, ..., N.$$

Finally, Eq. (4) is introduced into Eq. (5), yielding:

$$\mathbf{u}_{LB} = \mathbf{\Phi}_{LB}\mathbf{\Phi}^{-1}\mathbf{u}. \tag{6}$$

Matrix $\mathbf{\Phi}_{LB}\mathbf{\Phi}^{-1}$ is called the differentiation matrix in the nomenclature of the pseudospectral method. It contains the weights for the approximation of the differential operators, and with the aid of the vector of function values, it discretizes the left-hand sides of Eq. (1). The discrete form of Eq. (1) is as follows:

$$\mathbf{\Phi}_{LB}\mathbf{\Phi}^{-1}\mathbf{u} = \mathbf{q}, \tag{7}$$

where $\mathbf{q} = \begin{bmatrix} \mathbf{f} & \mathbf{g} \end{bmatrix}^T$ is the vector of function values at the interior and boundary nodes.

The numerical solution at the nodes is obtained from Eq. (7) as:

$$\mathbf{u} = \mathbf{\Phi}\,\mathbf{\Phi}_{LB}^{-1}\mathbf{q}. \tag{8}$$

It is clearly seen that the solution is conditioned by the invertibility of the $\mathbf{\Phi}_{LB}$ matrix. This issue has involved researchers' attention in several papers [9, 15]. From this information follows that although the invertibility is not guaranteed, the cases where the matrix is singular are very rare, and the method has been successfully applied to many problems in science and engineering. To ensure the solvability of the problem, the so-called symmetric collocation approach should be used [16].

3. Application to the interface problems

As with all pseudospectral approaches, the RBF-PS is well suited for problems possessing smooth solutions. To use the method's advantages in problems possessing weak discontinuities on interfaces, the method is implemented with the subdomain approach.

Let us assume that the domain of a heterogeneous problem can be divided into several subdomains, in the way that the problem is homogeneous in each of them. Without loss of generality we assume two such subdomains, as presented in Fig. 1.

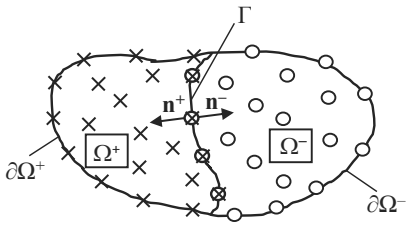

Fig. 1. The domain of the problem with node discretization.

Now the boundary-value problem (1) can be written as a subdomain problem in the following form:

$$\begin{aligned} L^+u^+ &= f^+ \quad \text{in} \quad \Omega^+, \qquad B^+u^+ = g^+ \quad \text{on} \quad \partial\Omega^+, \\ L^-u^- &= f^- \quad \text{in} \quad \Omega^-, \qquad B^-u^- = g^- \quad \text{on} \quad \partial\Omega^-. \end{aligned} \tag{9}$$

To make the problem well-posed, some continuity conditions on interface Γ have to be defined.

To accurately address the problem, two continuity conditions that ensure the continuity of the solution as well as the continuity of the flux or traction, dependently on the analyzed physical problem, have to be imposed on the interface [13, 14]. They can be put in general form as:

$$\begin{aligned} &u^+ - u^- = 0, \\ &T^+u^+ \cdot \mathbf{n}^+ + T^-u^- \cdot \mathbf{n}^- = 0, \qquad \text{on } \Gamma, \end{aligned} \tag{10}$$

where T denotes the respective differential operator, and $\mathbf{n}$ is the normal outward vector to the interface.

Next, the differentiation matrices have to be determined for each subdomain as well as for the interface, following the procedure from Sec. 2. The interpolation function takes the form:

$$u(\mathbf{x}) = \begin{cases} u^+(\mathbf{x}) = \sum_{j=1}^{N^+} \alpha_j^+ \varphi_j^+ \left(\left\| \mathbf{x} - \mathbf{x}_j^+ \right\| \right) & \mathbf{x}_j^+ \in \overline{\Omega}^+, \\ u^-(\mathbf{x}) = \sum_{j=1}^{N^-} \alpha_j^- \varphi_j^- \left(\left\| \mathbf{x} - \mathbf{x}_j^- \right\| \right) & \mathbf{x}_j^- \in \overline{\Omega}^-, \end{cases} \tag{11}$$

where $\overline{\Omega}^+ = \Omega^+ \cup \partial\Omega^+ \cup \Gamma$ and $\overline{\Omega}^- = \Omega^- \cup \partial\Omega^- \cup \Gamma$ represent the closed subdomains. Taking into account that the collocation procedure is used at the stage of determination of the differentiation matrices, two degrees of freedom should exist at the same position on the interface due to Eq. (10). It is fulfilled by the fact that this position is occupied by one node from $\overline{\Omega}^+$ as well as from $\overline{\Omega}^-$, as shown in Fig. 1.

The global discrete system can be written in the form of Eq. (7) but the matrices and vectors included in this equation have the following structure in the subdomain approach:

$$\boldsymbol{\Phi}_{LB} = \begin{bmatrix} \boldsymbol{\Phi}_{LB}^+ & \mathbf{0} \\ \mathbf{0} & \boldsymbol{\Phi}_{LB}^- \\ \boldsymbol{\Phi}_{\Gamma}^+ & -\boldsymbol{\Phi}_{\Gamma}^- \end{bmatrix}, \qquad \boldsymbol{\Phi} = \begin{bmatrix} \boldsymbol{\Phi}^+ & \mathbf{0} \\ \mathbf{0} & \boldsymbol{\Phi}^- \end{bmatrix},$$

$$\mathbf{u} = \begin{bmatrix} \mathbf{u}^+ \\ \mathbf{u}^- \end{bmatrix}, \qquad \mathbf{q} = \begin{bmatrix} \mathbf{f}^+ \\ \mathbf{g}^+ \\ \mathbf{f}^- \\ \mathbf{g}^- \\ \mathbf{0} \end{bmatrix}, \tag{12}$$

where $\boldsymbol{\Phi}_{LB}^+$ and $\boldsymbol{\Phi}_{LB}^-$ are the Kansa type matrices combined with differential operators L^+, B^+ and L^-, B^-, respectively. They are generated by the collocation at the internal ($\mathbf{x}_i^{I+}$, $\mathbf{x}_i^{I-}$) as well as the boundary nodes ($\mathbf{x}_i^{B^+}$, $\mathbf{x}_i^{B^-}$) from respective subdomains $\Omega^+ \cup \partial\Omega^+$ and $\Omega^- \cup \partial\Omega^-$, i.e.,

$$\boldsymbol{\Phi}_{LB}^+ = \begin{bmatrix} \boldsymbol{\Phi}_L^+ \\ \boldsymbol{\Phi}_B^+ \end{bmatrix}, \qquad \boldsymbol{\Phi}_{LB}^- = \begin{bmatrix} \boldsymbol{\Phi}_L^- \\ \boldsymbol{\Phi}_B^- \end{bmatrix},$$

where

$$\left(\boldsymbol{\Phi}_L^+\right)_{ij} = \left[L^+ \varphi^+ \left(\left\| \mathbf{x} - \mathbf{x}_j^+ \right\| \right) \right]_{\mathbf{x}=\mathbf{x}_i^{I+}}, \qquad i = 1, ..., N_I^+, \quad j = 1, ..., N^+,$$

$$\left(\boldsymbol{\Phi}_B^+\right)_{ij} = \left[B^+ \varphi^+ \left(\left\| \mathbf{x} - \mathbf{x}_j^+ \right\| \right) \right]_{\mathbf{x}=\mathbf{x}_i^{B+}}, \qquad i = 1, ..., N_B^+, \quad j = 1, ..., N^+,$$

$$\left(\mathbf{\Phi}_L^-\right)_{ij} = \left[L^-\varphi^-\left(\left\|\mathbf{x}-\mathbf{x}_j^-\right\|\right)\right]_{\mathbf{x}=\mathbf{x}_i^{I-}}, \qquad i=1,...,N_I^-, \quad j=1,...,N^-,$$

$$\left(\mathbf{\Phi}_B^-\right)_{ij} = \left[B^-\varphi^-\left(\left\|\mathbf{x}-\mathbf{x}_j^-\right\|\right)\right]_{\mathbf{x}=\mathbf{x}_i^{B-}}, \qquad i=1,...,N_B^-, \quad j=1,...,N^-.$$

Matrices $\mathbf{\Phi}_\Gamma^+$, $\mathbf{\Phi}_\Gamma^-$ are the Kansa type matrices reflecting the interface conditions included in Eq. (10). They are generated by the collocation at the interface nodes ($\mathbf{x}_i^\Gamma$), i.e.,

$$\mathbf{\Phi}_\Gamma^+ = \begin{bmatrix} \mathbf{\Phi}^+ \\ \mathbf{\Phi}_T^+ \end{bmatrix}, \qquad \mathbf{\Phi}_\Gamma^- = \begin{bmatrix} \mathbf{\Phi}^- \\ \mathbf{\Phi}_T^- \end{bmatrix},$$

where

$$\left(\mathbf{\Phi}^+\right)_{ij} = \varphi^+\left(\left\|\mathbf{x}_i^\Gamma-\mathbf{x}_j^+\right\|\right), \qquad i=1,...,N_\Gamma, \quad j=1,...,N^+,$$

$$\left(\mathbf{\Phi}_T^+\right)_{ij} = \left[T_n^+\varphi^+\left(\left\|\mathbf{x}-\mathbf{x}_j^+\right\|\right)\right]_{\mathbf{x}=\mathbf{x}_i^\Gamma}, \qquad i=1,...,N_\Gamma, \quad j=1,...,N^+,$$

$$\left(\mathbf{\Phi}^-\right)_{ij} = \varphi^-\left(\left\|\mathbf{x}_i^\Gamma-\mathbf{x}_j^-\right\|\right), \qquad i=1,...,N_\Gamma, \quad j=1,...,N^-,$$

$$\left(\mathbf{\Phi}_T^-\right)_{ij} = \left[T_n^-\varphi^-\left(\left\|\mathbf{x}-\mathbf{x}_j^-\right\|\right)\right]_{\mathbf{x}=\mathbf{x}_i^\Gamma}, \qquad i=1,...,N_\Gamma, \quad j=1,...,N^-.$$

In the above equation, the projection along the normal outward vector, according to Eq. (10), is included in differential operators T_n^+ and T_n^-.

Matrices $\mathbf{\Phi}^+$ and $\mathbf{\Phi}^-$ are the interpolation matrices that are generated using the nodes ($\mathbf{x}_i^+$, $\mathbf{x}_i^-$) from the appropriate closed subdomains $\overline{\Omega}^+$ and $\overline{\Omega}^-$, i.e.,

$$\left(\mathbf{\Phi}^+\right)_{ij} = \varphi^+\left(\left\|\mathbf{x}_i^+-\mathbf{x}_j^+\right\|\right), \qquad i,j=1,...,N^+,$$

$$\left(\mathbf{\Phi}^-\right)_{ij} = \varphi^-\left(\left\|\mathbf{x}_i^--\mathbf{x}_j^-\right\|\right), \qquad i,j=1,...,N^-.$$

Vector $\mathbf{u}$ includes unknown function values from respective closed subdomains and $\mathbf{q}$ is the right-hand-side vector. The above objects are complemented by zero matrices of appropriate size. It is the main structural difference of the discretized equation compared to the full matrices in conventional RBF-PS [8].

The solution of the interface problem can be represented by Eq. (8), where the objects from Eq. (12) are introduced. It is obvious that the existence and uniqueness of the solution are associated with the non-singularity of the Φ_{LB} matrix. Although, as mentioned in Sec. 2, the non-singularity of the Kansa type matrix is not guaranteed, the previous and present works do not indicate the cases where singularity appears.

4. Choice of the shape parameter in radial basis function

Most RBFs include a constant parameter that controls their flatness (shape parameter). The values of this parameter that cause the functions to be flattened theoretically increase the accuracy. Therefore, these functions have an advantage over other RBFs without this parameter. On the other hand, the system matrix generated with the use of flattened RBF has rows or columns almost linearly dependent, which means that the matrix is almost singular and the system is difficult to be solved numerically. This phenomenon is known as the uncertainty principle. Several papers have been devoted to this issue [17] and some algorithms for estimating a proper value of the shape parameter have been developed.

Among these algorithms, two most often used are tested in the present paper in the context of the subdomain approach. One of them takes into account the problems of numerical stability to estimate the value of the shape parameter, while the other focuses on accuracy of the problem under consideration.

4.1. Tracking of the condition number

To obtain the appropriate value of the parameter, a heuristics approach that relates numerical accuracy and stability with the number of significant digits assumed for computation is used. This approach, along with an observation that the most accurate results in computation with the RBF are achieved when the value of the condition number of the system matrix is sufficiently high, leads to the following expression:

$$\log_{10} \kappa(\mathbf{\Phi}_{LB}) \in [r_l, r_u] \Rightarrow \varepsilon^*, \tag{13}$$

which is the base for estimating the proper value of the shape parameter ε^*. In Eq. (13), κ denotes the condition number, and r_l and r_u are the lower and upper bounds of the range based on the number of significant digits (computational precision). Usually, r_u is 16 when one operates double precision and r_l is a little less. The algorithm determines the value of the shape parameter that makes the condition number of the system matrix sufficiently large while preserving stable computation. The details of the approach are explained in [18].

4.2. Leave-one-out algorithm

The leave-one-out approach comes from interpolation problems, but it was also used in RBF collocation techniques [3]. In this algorithm, an optimal value of the parameter is obtained by minimizing the error of the interpolant based on the data from which one of the nodes was "left out". The error at the k-th node, which was left out, can be obtained as:

$$E_k = u_k - u^{[k]}(\mathbf{x}_k), \tag{14}$$

where u_k is the function value at this node and

$$u^{[k]}(\mathbf{x}_k) = \sum_{\substack{j=1 \\ j\neq k}}^{N} \alpha_j^{[k]} \varphi\left(\|\mathbf{x}-\mathbf{x}_j\|\right)$$

is the RBF interpolant to the data $\mathbf{u} = [u_1, ..., u_{k-1}, u_{k+1}, ..., u_N]$.

By removing, in turn, each of the nodes, the vector of errors $\mathbf{E} = \begin{bmatrix} E_1 & \cdots & E_N \end{bmatrix}^T$ can be composed. The norm of this vector indicates the quality of the fit, which depends on the shape parameter. By repeating calculations for different values of the parameter, one can choose the optimal one, which minimizes the norm $\|\mathbf{E}\|$.

Since the implementation of this strategy is rather expensive, Rippa [19] showed that E_k could be computed in a simpler way as:

$$E_k = \frac{\alpha_k}{(\mathbf{\Phi}^{-1})_{kk}}, \tag{15}$$

where α_k is the k-th coefficient in the interpolant u based on the full set of nodes and $\mathbf{\Phi}^{-1}_{kk}$ is the k-th element in the diagonal of the inverse of the interpolation matrix.

The adaptation of this strategy to the RBF-PS is shown, e.g., in [20]. According to this, the error presented by Eq. (15) is computed as:

$$E_k = \frac{\alpha_k}{\left(\mathbf{\Phi}^{-1}_{LB}\right)_{kk}} = \frac{\left(\mathbf{\Phi}^{-1}_{LB} \cdot \mathbf{q}\right)_k}{\left(\mathbf{\Phi}^{-1}_{LB}\right)_{kk}}. \tag{16}$$

For the RBF-PS subdomain, the objects included in the above equation come from Eq. (12).

5. Numerical results

Several examples are solved to examine the usefulness of the presented method in solving the problems possessing weak discontinuities on interfaces. The results obtained lead to similar conclusions. Two of these examples are presented below. In the computation, the multiquadric RBF $\varphi_j(\mathbf{x}) = \sqrt{\varepsilon^2 \|\mathbf{x}-\mathbf{x}_j\|_2^2 + 1}$ is used, where ε is the shape parameter.

5.1. Diffusion between concentric cylinders

The first example describes diffusion in a cylindrical annulus with prescribed surface potential. The governing equation in cylindrical coordinates (r, θ, z) is as follows [21]:

$$\frac{D}{r}\frac{\partial}{\partial r}\left(r\frac{\partial \phi}{\partial r}\right) + \frac{D}{r^2}\frac{\partial^2 \phi}{\partial \vartheta^2} + D\frac{\partial^2 \phi}{\partial z^2} = 0, \qquad \phi(r_1) = 1, \quad \phi(r_2) = 2, \tag{17}$$

where $r_1 = 0.025$ and $r_2 = 1$. Assuming the axisymmetry and uniformity along the z coordinate, the equation can be simplified to ordinary differential one as follows:

$$D\frac{\partial^2\phi}{\partial r^2} + \frac{D}{r}\frac{\partial\phi}{\partial r} = 0 \tag{18}$$

and viewed as a steady, one-dimensional convection-diffusion problem.

It is assumed that the problem possesses two interfaces, where the diffusion parameter has some jumps. Its value is as follows:

$$D = \begin{cases} D^{(1)} = 1 & \text{for} \quad r \in [0.025, 0.25], \\ D^{(2)} = 0.1 & \text{for} \quad r \in (0.25,\ 0.5], \\ D^{(3)} = 0.01 & \text{for} \quad r \in (0.5, 1]. \end{cases} \tag{19}$$

The domain of the problem is shown in Fig. 2.

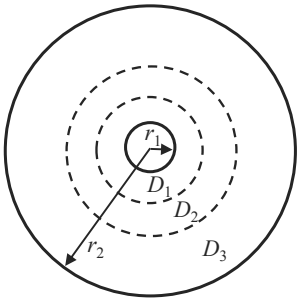

FIG. 2. The domain of the problem with two interfaces.

The continuity conditions at the interfaces are put in the following way:

$$\begin{aligned} &\phi^{(1)} - \phi^{(2)} = 0, \qquad D^{(1)}\phi^{(1)\prime} - D^{(2)}\phi^{(2)\prime} = 0 \qquad \text{at} \quad r = 0.25, \\ &\phi^{(2)} - \phi^{(3)} = 0, \qquad D^{(2)}\phi^{(2)\prime} - D^{(3)}\phi^{(3)\prime} = 0 \qquad \text{at} \quad r = 0.5. \end{aligned} \tag{20}$$

They ensure the continuity of the solution at the interface nodes as well as the continuity of the flux across the interfaces.

Since D coefficient has different values in adjacent subdomains, one can expect a non-smooth solution with a discontinuous derivative. The numerical solution and the exact one are presented in Fig. 3.

Since the method provides the solution as numerical values at the nodes a derivative of the solution can be obtained using Eq. (6) by inserting the matrix that discretizes the respective derivative instead of $\mathbf{\Phi}_{LB}$. The numerically computed first-order derivative of potential function φ and the exact one are shown in Fig. 4.

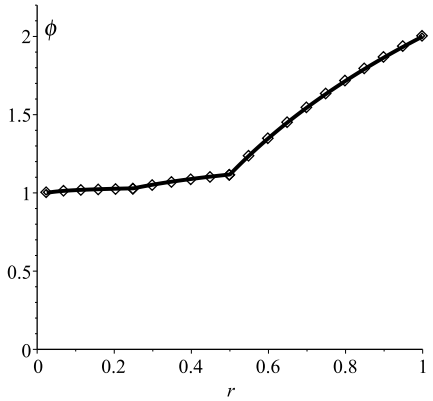

FIG. 3. Solution of the 1D convection-diffusion problem: numerical solution with $N = 23$ nodes uniformly distributed in each subdomain ($N^{(1)} = 6$, $N^{(2)} = 6$, $N^{(3)} = 11$) – discrete line, exact solution – solid line.

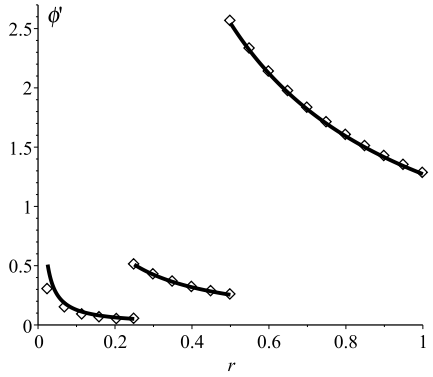

FIG. 4. Derivative of the solution: numerically obtained with $N = 23$ nodes uniformly distributed in each subdomain ($N^{(1)} = 6$, $N^{(2)} = 6$, $N^{(3)} = 11$) – discrete line, exact one – solid line.

From Figs. 3 and 4, one can conclude that a few nodes in each subdomain ensure acceptable accuracy. Due to the proper continuity conditions at the interfaces, accuracy is not destroyed near interface nodes.

The accuracy and stability of the solution process are strongly dependent on the number of nodes as well as on the value of the shape parameter. The influence of these factors on the accuracy is shown in Fig. 5a, where the root mean square error (RMS) of the solution vs. shape parameter is presented for certain node distributions. Figure 5b shows the influence of the shape parameter on the condition number of the system matrix for these node distributions.

The figures show that a larger number of nodes leads to higher accuracy. The highest accuracy for each of the assumed node distributions is achieved

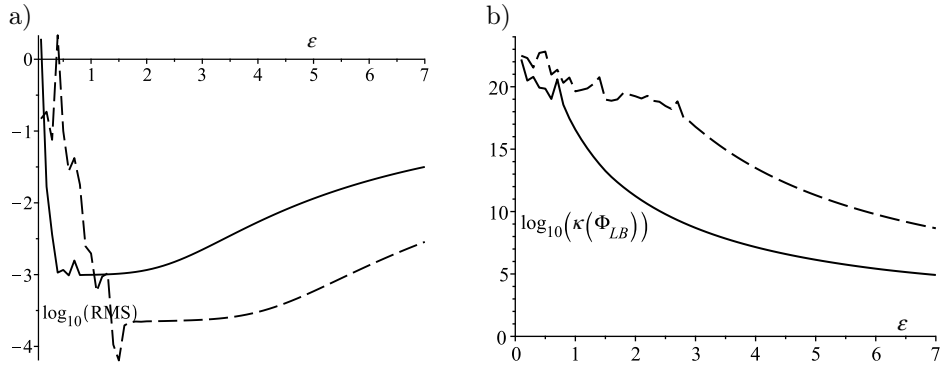

FIG. 5. Accuracy and stability of the solution of the 1D convection-diffusion problem: a) RMS vs. shape parameter; b) condition number of the system matrix vs. shape parameter; solid line: $N = 23$ nodes ($N^{(1)} = 6$, $N^{(2)} = 6$, $N^{(3)} = 11$), dash line: $N = 42$ nodes ($N^{(1)} = 10$, $N^{(2)} = 11$, $N^{(3)} = 21$).

in different regions of ε. It is strongly connected with the conditioning of the system.

Similarly, as in conventional use of the RBS-PS [3], also in the subdomain approach small values of the shape parameter that theoretically should provide the most accurate results lead to high inaccuracy due to a highly ill-conditioned system. In Fig. 5a there is a range of ε for a given number of nodes, where the results are the most accurate. In this range, the values of the condition number are close to the number of computational digits assumed for the computation (herein 16 – double precision). It indicates that the algorithm presented in Subsec. 4.1 can be successfully applied to estimate the proper value of the shape parameter also in the subdomain approach. The results of the application of the algorithms from Sec. 4 for the estimation of the proper value of ε are presented in Table 1. The table shows that these algorithms give values that lead to good accuracy, although the algorithm from Subsec. 4.1 exhibits better performance.

TABLE 1. Values of the shape parameter for the 1D convection-diffusion problem obtained by the algorithms from Sec. 4, corresponding RMS error and rate of convergence.

N	ε_{opt}	RMS with ε_{opt}	ε_1 (Subsec. 4.1)	RMS with ε_1	ε_2 (Subsec. 4.2)	RMS with ε_2
23	0.6	0.9752e-3	1.1	0.9972e-3	0.6	0.9752e-3
rate		–		–		–
42	1.5	0.6374e-4	3.3	0.2444e-3	1.1	0.5835e-3
rate		4.38		2.26		0.82
55	5.4	0.1833e-4	4.7	0.6142e-4	2.8	0.1014e-3
rate		4.52		5.01		6.35

5.2. 2D elliptic equation

As the second example, a two-dimensional elliptic equation of the form:

$$\begin{aligned} \nabla \cdot (\beta(\mathbf{x})\, \nabla u(\mathbf{x})) &= f(\mathbf{x}), \qquad \mathbf{x} = (x, y) \in \Omega, \\ u(\mathbf{x}) &= g(\mathbf{x}), \qquad x \in \partial\Omega \end{aligned} \tag{21}$$

is solved, where the diffusion coefficient has the following discontinuity:

$$\beta(\mathbf{x}) = \begin{cases} \beta^+ = 10, & \mathbf{x} \in \Omega^+, \\ \beta^- = 1, & \mathbf{x} \in \Omega^-. \end{cases} \tag{22}$$

In this case, the interface conditions that ensure the continuity of the solution on the interface and the continuity of the flux across the interface assume the form:

$$\begin{aligned} &u^+ - u^- = 0, \\ &\beta^+ \frac{\partial u^+}{\partial n} - \beta^- \frac{\partial u^-}{\partial n} = 0, \quad \text{on } \Gamma, \end{aligned} \tag{23}$$

where the derivative is computed in the direction of the normal outward vector to the interface.

The configuration of the subdomains with sample node distribution is presented in Fig. 6.

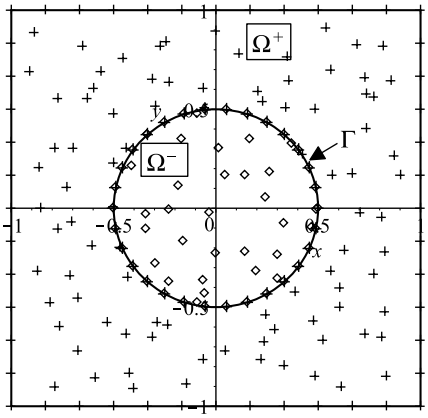

Fig. 6. The domain configuration with an irregular (pseudorandom) node distribution.

The solution of the problem by the subdomain RBF-PS method is presented in Fig. 7, along with the exact solution. The figure confirms that by using the method with proper interface conditions one can expect good accuracy.

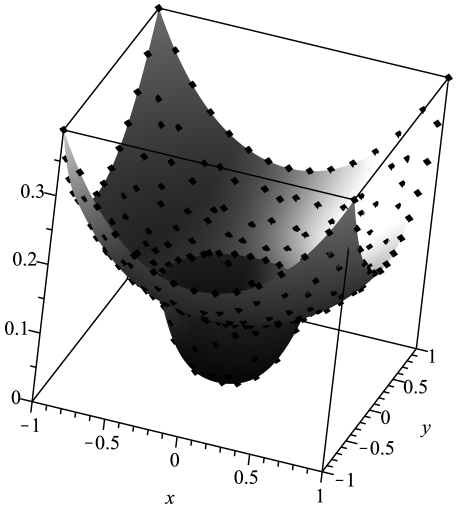

FIG. 7. Numerical solution of the 2D elliptic equation with $N = 285$ irregularly distributed nodes ($N^+ = 216$, $N^- = 69$) along with the exact solution.

The influence of the shape parameter and the number of nodes on the accuracy as well as on the stability is presented in Fig. 8.

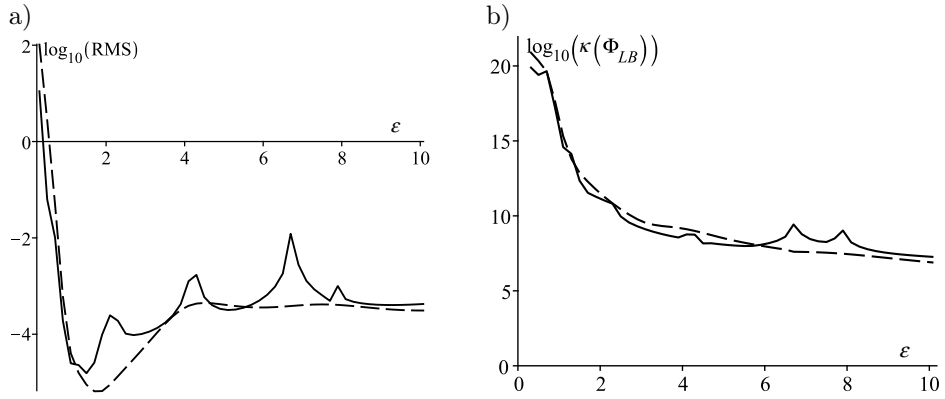

FIG. 8. Accuracy and stability of the solution of the 2D elliptic equation: a) RMS vs. shape parameter; b) condition number of the system matrix vs. shape parameter; solid line: $N = 285$ pseudo randomly distributed nodes ($N^+ = 216$, $N^- = 69$), dash line: $N = 349$ pseudo-randomly distributed nodes ($N^+ = 267$, $N^- = 82$).

The main conclusions from the analysis of the results presented in Fig. 8 are similar to those drawn from the 1D example. Table 2 shows values of the shape parameter determined for the 2D elliptic problem by the algorithms mentioned in the present paper.

TABLE 2. Values of the shape parameter for the 2D elliptic problem obtained by the algorithms from Sec. 4, corresponding RMS error and rate of convergence.

N	ε_{opt}	RMS with ε_{opt}	ε_1 (Subsec. 4.1)	RMS with ε_1	ε_2 (Subsec. 4.2)	RMS with ε_2
285 irregular	1.5	0.1550e-4	1.1	0.2490e-4	1.7	0.2569e-4
rate		–		–		–
349 irregular	1.7	0.6540e-5	1.3	0.1575e-4	2.1	0.8960e-5
rate		4.25		2.26		5.19
285 uniform	2.1	0.1731e-4	1.1	0.3053e-4	1.5	0.2153e-4
rate		–		–		–
349 uniform	1.5	0.1180e-4	1.3	0.1520e-4	1.3	0.1520e-4
rate		1.90		3.44		1.50

The results presented in Table 2 indicate that both algorithms are effective when estimating the proper value of the shape parameter for the RBF-PS method in the subdomain approach, leading to similar accuracy.

6. Conclusions

In this study, the formulation of the RBF-PS method used in the subdomain approach was developed. The method can handle the problems possessing weak discontinuity on the interface, maintaining the main advantages of the global RBF collocation methods, such as: meshless character, high rate of convergence (a few nodes are sufficient to achieve high accuracy), simplicity of the implementation. Due to physically justified interface conditions, the method gives very accurate results. An important issue when applying RBF collocation methods is estimating the proper value of the shape parameter for the RBF. In the RBF-PS subdomain method, the structures of the matrices in discretized equation differ from those in the classical method. They possess some blocks of zero matrices, and therefore they are not as dense as in the conventional method. Therefore, an important question arises whether the algorithms used in conventional RBF collocation methods for estimating the shape parameter value are also effective in the subdomain RBF-PS. Based on the examples of one- and two-dimensional equations, it was found that these algorithms can also be successfully applied in the subdomain approach.

References

1. T. Belytschko, Y. Krongauz, D. Organ, M. Fleming, P. Krysl, Meshless methods: an overview and recent developments, *Computer Methods in Applied Mechanics and Engineering*, **139**(1–4): 3–47, 1996, doi: 10.1016/S0045-7825(96)01078-X.

2. G.R. Liu, *Mesh Free Methods, Moving Beyond the Finite Element Method*, CRC Press, Boca Raton, USA, 2003.

3. G.E. Fasshauer, *Meshfree Approximation Methods with Matlab*, World Scientific Publishing, Singapore, 2007.

4. M.D. Buhmann, *Radial Basis Functions: Theory and Implementations*, Cambridge University Press, Cambridge, UK, 2003.

5. W.R. Madych, Miscellaneous error bounds for multiquadric or related interpolators, *Computers & Mathematics with Applications*, **24**(12): 121–138, 1992, doi: 10.1016/0898-1221(92)90175-H.

6. E.J. Kansa, Multiquadrics – A scattered data approximation scheme with applications to computational fluid-dynamics – I: Surface approximations and partial derivative estimates, *Computers & Mathematics with Applications*, **19**(8–9): 127–145, 1990, doi: 10.1016/0898-1221(90)90270-T.

7. E.J. Kansa, Multiquadrics – A scattered data approximation scheme with applications to computational fluid dynamics – II: Solutions to parabolic, hyperbolic, and elliptic partial differential equations, *Computers & Mathematics with Applications*, **19**(8–9): 147–161, 1990, doi: 10.1016/0898-1221(90)90271-K.

8. A. Krowiak, Radial basis function-based pseudospectral method for static analysis of thin plates, *Engineering Analysis with Boundary Elements*, **71**: 50–58, 2016, doi: 10.1016/j.enganabound.2016.07.002.

9. W. Chen, Z.-J. Fu, C.S. Chen, *Recent Advances in Radial Basis Function Collocation Methods*, Springer, 2014.

10. B. Martin, B. Fornberg, Using radial basis function-generated finite differences (RBF-FD) to solve heat transfer equilibrium problems in domains with interfaces, *Engineering Analysis with Boundary Elements*, **79**: 38–48, 2017, doi: 10.1016/j.enganabound.2017.03.005.

11. A. Taleei, M. Dehghan, An efficient meshfree point collocation moving least squares method to solve the interface problems with nonhomogeneous jump conditions, *Numerical Methods for Partial Differential Equations*, **31**(4): 1031–1053, 2015, doi: 10.1002/num.21935.

12. A. Taleei, M. Dehghan, Direct meshless local Petrov–Galerkin method for elliptic interface problems with applications in electrostatic and elastostatic, *Computer Methods in Applied Mechanics and Engineering*, **278**: 479–498, 2014, doi: 10.1016/j.cma.2014.05.016.

13. A. Krowiak, R. Filipowska, Kansa method for problems with weak discontinuity, [in:] AIP Conference Proceedings: 16th International Conference of Numerical Analysis and Applied Mathematics – ICNAAM 2018, 2116: 450021, 2019, doi: 10.1063/1.5114488.

14. Siraj-ul-Islam, M. Ahmad, Meshless analysis of elliptic interface boundary value problems, *Engineering Analysis with Boundary Elements*, **92**: 38–49, 2018, doi: 10.1016/j.enganabound.2017.07.008.

15. Y.C. Hon, R. Schaback, On nonsymmetric collocation by radial basis functions, *Applied Mathematics and Computation*, **119**(2–3): 177–186, 2001, doi: 10.1016/S0096-3003(99)00255-6.

16. Z.-M. Wu, Hermite–Birkhoff interpolation of scattered data by radial basis functions, *Approximation Theory and its Applications*, **8**: 1–10, 1992, doi: 10.1007/BF02836101.

17. R. Schaback, Error estimates and condition numbers for radial basis function interpolation, *Advances in Computational Mathematics*, **3**: 251–264, 1995, doi: 10.1007/BF02432002.

18. A. Krowiak, Domain-type RBF collocation methods for biharmonic problems, *International Journal of Computational Methods*, **15**(8): 1850078-1–1850078-20, 2018, doi: 10.1142/S0219876218500780.

19. S. Rippa, An algorithm for selecting a good value for the parameter c in radial basis function interpolation, *Advances in Computational Mathematics*, **11**: 193–210, 1999, doi: 10.1023/A:1018975909870.

20. A. Krowiak, J. Podgórski, The adaptation of the cross validation approach for RBF-based collocation methods, *Technical Transactions*, **7**: 147–156, 2017, doi: 10.4467/2353737XCT.17.115.6656.

21. D. Stevens, H. Power, M. Lees, H. Morvan, A local Hermitian RBF meshless numerical method for the solution of multi-zone problems, *Numerical Methods for Partial Differential Equations*, **27**(5): 1201–1230, 2011.

Received January 5, 2022; revised version April 20, 2022;
accepted May 19, 2022